



HAL
open science

Classical molecular dynamics study of small samples of amorphous silica: structural and dynamical properties

Mbaye Ndour, Laurent Chaput, Philippe Jund

► To cite this version:

Mbaye Ndour, Laurent Chaput, Philippe Jund. Classical molecular dynamics study of small samples of amorphous silica: structural and dynamical properties. *Journal of Non-Crystalline Solids*, 2021, 569, pp.120995. 10.1016/j.jnoncrysol.2021.120995 . hal-03266309

HAL Id: hal-03266309

<https://hal.science/hal-03266309>

Submitted on 2 Aug 2023

HAL is a multi-disciplinary open access archive for the deposit and dissemination of scientific research documents, whether they are published or not. The documents may come from teaching and research institutions in France or abroad, or from public or private research centers.

L'archive ouverte pluridisciplinaire **HAL**, est destinée au dépôt et à la diffusion de documents scientifiques de niveau recherche, publiés ou non, émanant des établissements d'enseignement et de recherche français ou étrangers, des laboratoires publics ou privés.



Distributed under a Creative Commons Attribution - NonCommercial 4.0 International License

Classical molecular dynamics study of small samples of amorphous silica : structural and dynamical properties

Mbaye Ndour,¹ Laurent Chaput,² and Philippe Jund¹

¹*ICGM - Université de Montpellier, CNRS, ENSCM, UMR 5253,
Place Eugène Bataillon, 34095 Montpellier Cedex 5, France*
²*LEMETA - Université de Lorraine, CNRS, UMR 7563,
2 avenue de la Forêt de Haye, 54518 Vandœuvre Cedex, France*

Ten small size samples of amorphous silica containing 78 atoms have been prepared using classical molecular dynamics and the van Beest-Kramer-van Santen (BKS) empirical potential. Our final goal is to use such samples in a forthcoming publication to compute accurately the thermal properties of silica from first principles calculations. The structural characteristics of these ten samples are in good agreement with experimental data. Dynamical properties, like the mean-square displacement, the vibrational density of states or the dynamic structure factor, have also been investigated and compare relatively well with data from neutron scattering experiments. These small dynamically stable structures can therefore be used subsequently to study more complicated physical properties, like the thermal conductivity or the diffusivity at a reduced computational cost.

I. INTRODUCTION

In the last decades, amorphous silica has attracted considerable interest in diverse technological applications, including microelectronic devices¹, optical fibers² and in many fields of science such as physics, chemistry and geology. It is considered as the archetypal network glass. Its structural³⁻¹¹ and dynamical¹²⁻²¹ properties have been extensively studied both theoretically⁸⁻¹⁷ and experimentally^{4-7,18-21}, but persistent challenges remain. Many computer-simulation-based structural models have been performed for creating realistic structural models of amorphous silica. The quality of a structural model depends generally on the choice of the interatomic potential. Different potentials have been used to model the structure of amorphous silica and the major differences between them can be found in the medium and long-range order. The parameters describing the former, mainly the Si-O-Si dihedral angle distribution, show some variations, not only in theoretical studies but also in experiments²². The subject of the determination of the amorphous structure of silica is thus very complex and continues to be an object of study.

The complexity of the structure is also reflected in the dynamics of the system. The characterization of the dynamical properties requires accurate calculations to determine exactly the excitations of the system. Theoretical approaches based on molecular-dynamics simulations are often used to study the dynamical properties but the deviations from experimental measurements are noticeable in particular in the case of the determination of the vibrational density of states (VDOS)^{13,14}. The difficulty to reproduce accurately the dynamical properties of amorphous silica can have origins in the incertitude on the structural model, the small size of the model or the imperfect empirical interatomic potentials. To get around the problem related to the flaws of an empirical potential, first-principles approaches have been used and the improvement of the results is remarkable^{12,17}.

In this paper we focus on the structural and dynamical properties of amorphous silica. Our goal is to produce small enough atomic structures to allow us to study physical properties at the level of Density Functional Theory (DFT) in forthcoming publications. The structures we would like to obtain should therefore be small enough, for those computations to be performed, but at the same time represent correctly the structural disorder, and be dynamically stable (i.e no imaginary phonon modes) for the empirical potential used in molecular dynamics, but at the DFT level as well. Those requirements are difficult to satisfy simultaneously since disorder is best described using large computational cells, and imaginary phonon modes may easily appear when periodic boundary conditions are applied. Nevertheless, we succeeded to build such minimal models of silica using simulation cells of 78 atoms which fulfill all the above mentioned constraints. Periodic boundary conditions have been used in our molecular dynamics studies to be compatible with the forthcoming ab initio calculations, since most DFT codes rely on their use.

Ten such structural models have been generated using molecular dynamics simulations which reproduce well the experimentally determined structure. By diagonalizing the dynamical matrix, we obtain the vibrational eigenfrequencies and eigenvectors that allow us to compute the dynamical properties of the different models. The calculated mean-square displacements and the vibrational density of states are compared with experiments. The dynamic structure factor is evaluated in the one-phonon approximation, as well as the effective neutron vibrational density of states. The latter is compared to the experimental vibrational density of states and reasonably good results are obtained.

This paper is organized as follows: in section II we describe the computer simulations used to generate the models. Section III gives the structural properties of the models. The dynamical properties are calculated in section IV. Conclusions are given in section V

II. GENERATION OF SILICA GLASSES

In this study we consider SiO_2 glasses which are described at a given temperature using classical molecular dynamics simulations with the so-called BKS potential²³. This potential describes the interactions between atoms according to the formula,

$$U(r_{ij}) = \frac{q_i q_j e^2}{r_{ij}} + A_{ij} \exp(-B_{ij} r_{ij}) - \frac{C_{ij}}{r_{ij}^6}, \quad (1)$$

where r_{ij} is the interparticle distance, e the charge of an electron and q_i , q_j , A_{ij} , B_{ij} and C_{ij} are parameters. These parameters are given in²⁴. The BKS potential is one the most widely used empirical potentials for silica because it describes very well the structural and vibrational properties of silica. An inconvenience in the BKS potential is that at short distance it can lead to an unphysical collapse of ions at high temperatures. In order to avoid unphysical energies at short distances, this functional form is often modified by adding a strongly repulsive term. We use in this study the short range repulsive term introduced by Jund et al.²⁴.

To obtain a statistical description of amorphous silica, we consider 10 SiO_2 samples, each one containing 78 atoms, 26 silicon, and 52 oxygen, confined in a cubic box with an edge length of 10.558 Å. This correspond to a mass density of 2.204 g/cm³ close to the experimental density ($\approx 2.2 \text{ g/cm}^3$). Periodic boundary conditions are used, and the long-range electrostatic forces are handled using the Ewald summation. As explained in a previous study²⁵, those 78 atoms structures are extracted from a supercell containing 648 atoms of β -cristobalite which has been melted at 5000 K to obtain a liquid. In order to obtain dynamically stable configurations, we carried out the heating, annealing and cooling processes using classical molecular dynamics simulations within the microcanonical ensemble. All systems are heated up to 7000 K and relaxed during 350 ps using a time steps of 0.7 fs. These liquid samples are then quenched to 300 K at a quenching rate of $2.6 \cdot 10^{11}$ K/s. After the quench, the atomic configurations are located in a basin around a local minimum. This local minimum is finally reached using a conjugate gradient algorithm. The procedure is summarized in Fig. 1.

III. STRUCTURAL PROPERTIES

A. Pair correlation functions

Bond length is one of the structural characteristics that we analyze to check that our amorphous silica structures are compatible with experiments. Pair correlation functions have been calculated to know informations about the bond length between nearest neighbors. The pair

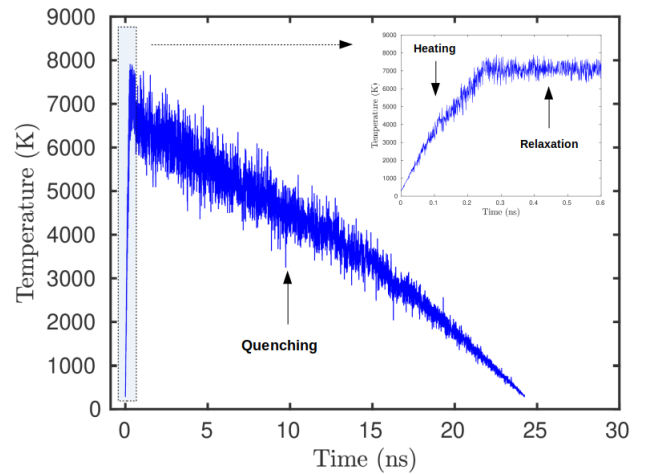


Figure 1: Temperature profile as a function simulation time in nanoseconds.

correlation functions can be expressed as follow¹⁶

$$g_{\alpha\beta}(r) = \frac{1}{N_{\alpha}\rho_{\beta}} \sum_{i \in \alpha, i' \in \beta} \delta(r - |\mathbf{R}_{i'} - \mathbf{R}_i|) \quad (2)$$

where N_{α} is the number of particles of type α , \mathbf{R}_i the position vector of atom i and ρ_{β} the average density of atoms of species β .

The results obtained from the calculation of these functions are plotted in Fig. 2. The average first pair distances corresponding to the first peaks are 3.18 Å, 1.63 Å and 2.64 Å for the Si-Si, Si-O and O-O distances respectively. These values are consistent with previous classical molecular dynamics results in²⁵, (3.21 Å, 1.62 Å and 2.66 Å). The authors of²⁵ also performed ab initio molecular-dynamics simulations and the average Si-Si distance that they found is smaller than our results (3.08 Å). This can be explained by the lack of a Si-Si short-range attraction term in the BKS potential. First-principles calculations⁸ performed on smaller samples (72 atoms) of amorphous silica have also shown smaller values for the Si-Si distances (3.1 Å) compared to those found with the BKS potential (3.12 Å). A densification can also decrease the Si-Si pair distances. This has been recently experimented by Trease et al.⁷.

One important parameter is the area under the first Si-O peak. It gives the number of oxygen atoms coordinated to the silicon atoms. Its calculated value is equal to four in this study, indicating a perfect chemical short-range order made of the expected structural units (SiO_4 tetrahedra).

B. Bond angle distribution

In this section, we quantify the dihedral angle (Si-O-Si) and the tetrahedral angle (O-Si-O) distributions which

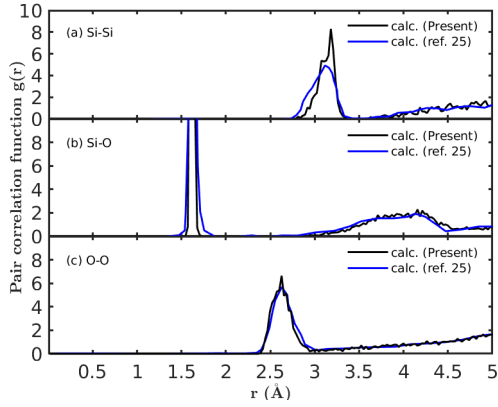


Figure 2: Pair correlation functions for Si-Si (upper graph), Si-O (middle graph) and O-O (lower graph). Our results are compared to the ab initio calculations performed in²⁵

are important for the validation of the structural analysis. Results for the bond angle distributions of the 10 samples are reported in Fig. 3 and Fig. 4 for the O-Si-O and Si-O-Si bond angle respectively. The broad Si-O-Si bond-angle distribution ranges from 120° to 180° . The lower limit and the upper limit of the range are similar to those found in the experimental results of⁴. The angular distribution is different from one structure to another and this difference can be interpreted by the topology of their structures, for instance, their ring size distribution²⁶. For each sample the mean Si-O-Si bond angle on different structures is within the range 150.74° - 154.82° . This result is close to the experimental value measured (152°) by da Silva et al.³ and the same value is obtained by Yan et al.²² in molecular dynamics simulation using the BKS potential. Indeed, the average Si-O-Si bond angle varies in different experimental measurements⁴⁻⁶ as well as in computer simulations^{17,25,27}. The average O-Si-O bond angle of our calculated structures is within the range 109.40° - 109.49° . This is in good agreement with the tetrahedral angle of 109.47° . This indicates that, as expected, Si centered tetrahedra are the structural units in all the systems.

C. Elastic structure factor

The elastic structure factor $S_{el}(Q)$ can be obtained by neutron scattering experiments when no energy is exchanged between the neutrons and the sample. In the harmonic approximation, it is given by²⁸

$$S_{el}(\mathbf{Q}) = \frac{1}{N\langle b^2 \rangle} \sum_{ij} \bar{b}_i \bar{b}_j e^{-(W_i + W_j)} e^{i\mathbf{Q} \cdot (\mathbf{R}_i - \mathbf{R}_j)}, \quad (3)$$

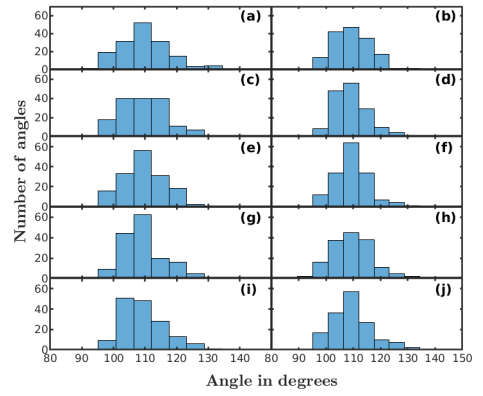


Figure 3: O-Si-O bond angle distribution of 10 structural models of amorphous silica

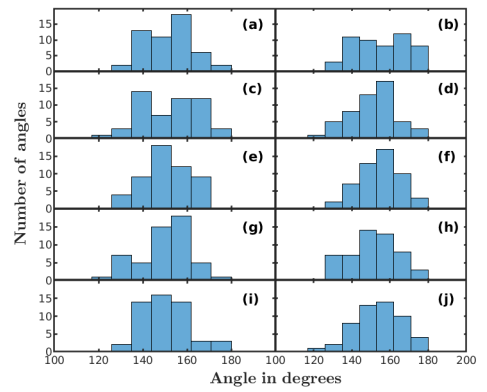


Figure 4: Si-O-Si bond angle distribution of 10 structural models of amorphous silica

where

$$\langle \bar{b}^2 \rangle = \frac{1}{N} \sum_i \bar{b}_i^2. \quad (4)$$

b_i is the neutron scattering length of atom i (the over-bar indicates averages over spin and isotope distributions for that element), \mathbf{Q} is the momentum transfer, N the number of atoms in the system and W_i the Debye-Waller factor defined by,

$$W_i(\mathbf{Q}) = \frac{1}{2} \langle (\mathbf{Q} \cdot \mathbf{u}_i)^2 \rangle. \quad (5)$$

For isotropic systems, Eq. (5) can be replaced by

$$W_i(\mathbf{Q}) = \frac{1}{6} Q \langle \mathbf{u}_i^2 \rangle. \quad (6)$$

In this equation, $\langle \mathbf{u}_i^2 \rangle$ is the mean squared displacement of atom i around the equilibrium position and the bracket denotes an average in a canonical ensemble, or time averaged if ergodicity is assumed.

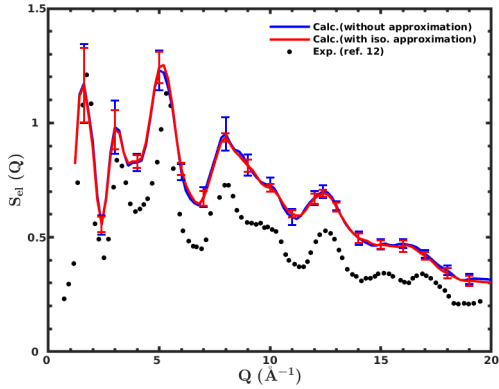


Figure 5: Elastic structure factor vs momentum transfer for amorphous silica calculated using the isotropic approximation (red solid line) and without this approximation (blue solid line) compared to experimental data¹²

To compare with experiments, it is the average of Eq. (5) over the \mathbf{Q} directions which is needed. We have performed this computation using 16200 directions, uniformly distributed over the solid angle. The results are shown in Fig. 5 as a blue line. They are in good agreement with experiments, which gives us confidence in our structural model. The elastic structure factor has also been calculated using the isotropic approximation (Eq. 6) and the results are shown as a red line. They are very similar to the exact calculation. It can be noted that our theoretical calculations overestimate the experimental results. This can be explained by a too large Debye-Waller factor since our computed mean-square displacement, $\langle u^2 \rangle = 0.0092 \text{ \AA}^2$, underestimates the measured one, $\langle u^2 \rangle = 0.0126 \text{ \AA}^2$.

IV. DYNAMICAL PROPERTIES

A. A. Vibrational density of states

The vibrational density of states (VDOS) allows to obtain information about the atomic dynamics. The basic ingredient needed to calculate it is the dynamical matrix which, in the harmonic approximation, can be expressed as,

$$D_{i\alpha i'\beta} = \frac{1}{\sqrt{m_i m_{i'}}} \frac{\partial^2 E}{\partial x_{i\alpha} \partial x_{i'\beta}}, \quad (7)$$

where m_i is the mass of atom i , α and β are cartesian directions, and indices i and i' run over the atoms in the system. In this study, because we use periodic boundary conditions, we have adopted the approach used for a crystal to obtain the dynamical properties. In this case,

the real space dynamical matrix is Fourier transformed over the periodic cell lattice vectors to obtain

$$D_{i\alpha i'\beta}(\mathbf{q}) = \frac{1}{\sqrt{m_i m_{i'}}} \sum_{l'} \frac{\partial^2 E}{\partial x_{0i\alpha} \partial x_{l'i'\beta}} e^{i\mathbf{q}(\mathbf{R}_{l'i'}^o - \mathbf{R}_{0i}^o)}, \quad (8)$$

where \mathbf{R}_{li}^o is the equilibrium position of atom i in the cell l . The vibrational modes are then obtained by solving the eigenvalue problem

$$\sum_{i'\beta} D_{i\alpha i'\beta}(\mathbf{q}) e_{\mathbf{q}j}^{i'\beta} = \omega_{\mathbf{q}j}^2 e_{\mathbf{q}j}^{i\alpha}, \quad (9)$$

\mathbf{q} is the wave vector, j is the band index and $\omega_{\mathbf{q}j}$ and $e_{\mathbf{q}j}^{i\alpha}$ represent the phonon frequency and its eigenmode respectively.

In this study, we have used the Phonopy package²⁹ to compute these quantities. To calculate the force constants, we have chosen $2 \times 2 \times 2$ supercells containing 624 atoms. The normalized vibrational density of states can be calculated from the obtained eigenfrequencies,

$$g(\omega) = \frac{1}{3NN_q} \sum_{\mathbf{q}j} \delta(\omega - \omega_{\mathbf{q}j}), \quad (10)$$

where N is the number of atoms in the cell and N_q the number of \mathbf{q} points sampled in the reciprocal space. We have used a $10 \times 10 \times 10$ \mathbf{q} -point sampling mesh. The function $g(\omega)$ is shown in Fig. 6. where we have replaced the delta function by a Gaussian function with a standard deviation $\sigma = 2.5 \text{ meV}$ (0.6 THz).

The vibrational spectrum shown in Fig. 6 shows two bands separated by a pseudo gap, a wide band in the frequency domain between 0 and ~ 25 THz and another band around 30-40 THz with a peak splitting at 35 THz. Similar results were obtained by Taraskin and Elliott¹³ (red solid curve in Fig. 6) using the BKS potential as well. However, comparison with experiments shows that with this potential the intermediate frequency region is badly described and in particular it is not possible to obtain the peak around 12 THz. This peak is indeed observed in experiments^{19,20} but also in first-principles calculations^{17,30}. Therefore it should be interpreted as a limit of the BKS potential as shown in³¹. The origin of the splitting in the high-frequency domain, found in amorphous silica, and other amorphous materials¹⁶, in experiments and in simulations, is analysed in the literature. Two origins are discussed. In¹³ it is related to the stretching of SiO_4 units, with an A_1 antisymmetric stretching significant only in the upper peak. On the other hand, the authors of³² prefer to see this splitting as an LO-TO splitting.

The total vibrational density of states can be decomposed as a sum of atomic contributions,

$$g_\alpha(\omega) = \frac{1}{3NN_q} \sum_{i \subset \alpha} \sum_{\mathbf{q}j} |e_{\mathbf{q}j}^i|^2 \delta(\omega - \omega_{\mathbf{q}j}), \quad (11)$$

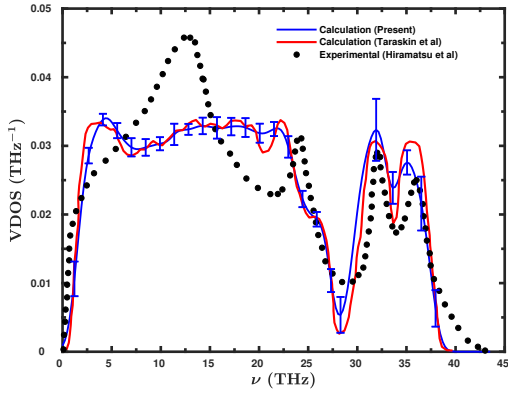


Figure 6: Vibrational density of states averaged over 10 model structures of amorphous silica (blue solid line) compared to data from experiments²⁰ (black points) and theory¹³ (red solid line).

where i runs over all atoms of type α and $\mathbf{e}_{\mathbf{q}j}^i$ are the components of eigenmode $\mathbf{q}j$ on atom i .

The partial vibrational density of states relative to the contribution of Si atoms and O atoms are reported in Fig. 7. The oxygen atoms dominate the spectrum below and above the pseudo gap, while the silicon atoms dominate around 25THz. This situation is analogous to the one observed in α -quartz³³.

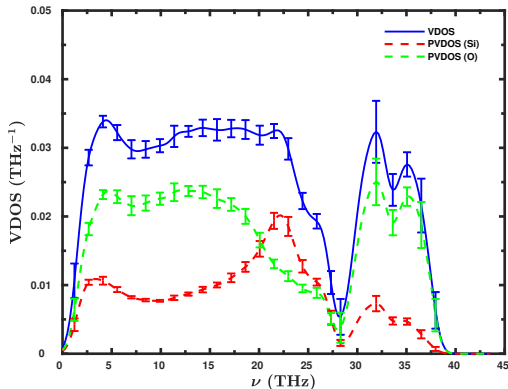


Figure 7: Partial vibrational density of states averaged over 10 model structures of amorphous silica for Si (red dashed line) and O (green dashed line) compared to the total VDOS (blue solid line). The standard deviations are also indicated by vertical lines.

B. Mean-square displacement

The mean-square displacement can be expressed in terms of eigenfrequencies and eigenvectors as³⁴,

$$\langle \overline{\mathbf{u}_i^2} \rangle = \frac{1}{N_q} \sum_{\mathbf{q}j} \frac{\hbar |\mathbf{e}_{\mathbf{q}j}^i|^2}{2m_i \omega_{\mathbf{q}j}} (2n_{\mathbf{q}j} + 1), \quad (12)$$

where $n_{\mathbf{q}j}$ is the Bose Einstein occupation function. In the following we compute this quantity for all the atoms in the system, and plot its average for the different species.

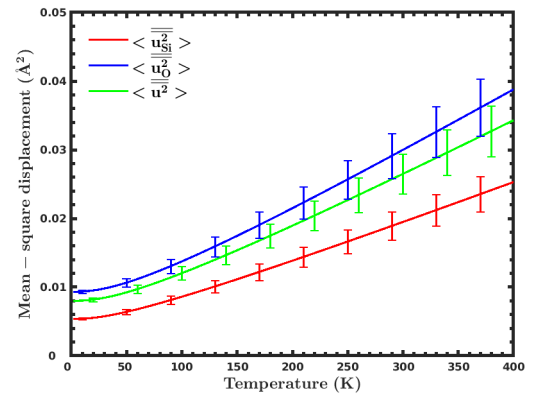


Figure 8: Mean-square displacement averaged over all the structures as a function of temperature for Si atoms (red solid line), O atoms (blue solid line) and all atoms in the system (green solid line)

The mean-square displacements calculated for each sample and averaged over all these samples for silicon and oxygen atoms are reported in Fig. 8. Our results at 33K, $\langle \overline{\mathbf{u}^2} \rangle = 0.0085 \pm 0.0003 \text{ \AA}^2$ compare well with experiments²⁸ $\langle \overline{\mathbf{u}^2} \rangle = 0.0073 \text{ \AA}^2$. At 300K the agreement of our calculations, $\langle \overline{\mathbf{u}^2} \rangle = 0.0265 \pm 0.003 \text{ \AA}^2$, with experiments is less obvious since several values are reported. $\langle \overline{\mathbf{u}^2} \rangle = 0.0285 \text{ \AA}^2$ by Nakamura et al.²¹ and $\langle \overline{\mathbf{u}^2} \rangle = 0.0121 \text{ \AA}^2$ by Wright and Sinclair³⁵. Nevertheless our calculated results agree well with the ones of Taraskin and Elliott¹³ who also used the BKS potential.

C. Dynamic structure factor and effective neutron density of states

The dynamic structure factor is proportional to the double differential cross-section, and therefore can be obtained from neutron measurements. For SiO_2 it reduces to the coherent part since for silicon and oxygen the incoherent contribution is negligible. In the one-phonon

approximation²⁸, it is given by

$$S(\mathbf{Q}, \omega) = \frac{1}{N_q N \langle b^2 \rangle} \sum_{ii'} \bar{b}_i \bar{b}_{i'} e^{-(W_i + W_{i'})} e^{i\mathbf{Q} \cdot (\mathbf{R}_{i'} - \mathbf{R}_i)} \\ \times \sum_{\mathbf{qj}} \frac{(\mathbf{Q} \cdot \mathbf{e}_{\mathbf{qj}})^* (\mathbf{Q} \cdot \mathbf{e}_{\mathbf{qj}}^i)}{2(m_i m_{i'})^{1/2}} [n_{\mathbf{qj}} + 1] \delta(\omega - \omega_{\mathbf{qj}}). \quad (13)$$

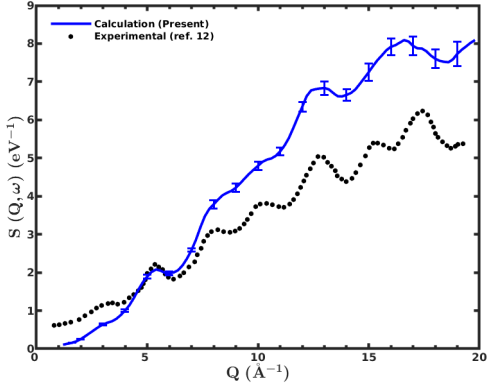


Figure 9: Average dynamic structure factor vs momentum transfer for $\nu = 3.02$ THz compared with experiment¹².

As for the elastic structure factor, to be compared to experiments, the above quantity should be averaged over the \mathbf{Q} directions. The result of this calculation is compared with experiments in Fig. 9 for $\nu = 3.02$ THz. The relative agreement that we obtain supports the use of our structural models to study the dynamical properties of silica.

The previous figure focuses on the Q dependence of the dynamic structure factor at fixed frequency. To study the ω dependence, the effective neutron density of states is usually employed. It is defined by²⁸

$$G(\omega) = \frac{\int_{Q_1}^{Q_2} G(Q, \omega) dQ}{Q_2 - Q_1}, \quad (14)$$

$$G(Q, \omega) = \frac{2\bar{m}\omega}{\hbar Q^2 e^{-2\bar{W}} [n(\omega, T) + 1]} S(Q, \omega), \quad (15)$$

where $\bar{m}^{-1} = \sum_i m_i^{-1}/N$ and $\bar{W} = Q^2 \langle u^2 \rangle / 6$ with $\langle u^2 \rangle$ the average of the mean-square displacements over all atoms.

Figure 10 shows a comparison between our calculations and data from experiments^{19,36}. The calculation of the effective neutron density of states according to Eq. (14) was done at a temperature of 2 K. The average over Q was performed in the range 6-13 \AA^{-1} , corresponding to the range in the experiment of Carpenter and Price¹⁹. At low-frequency, the theoretical curve follows the results of the experiment of Buchenau et al.³⁶. The peak, which

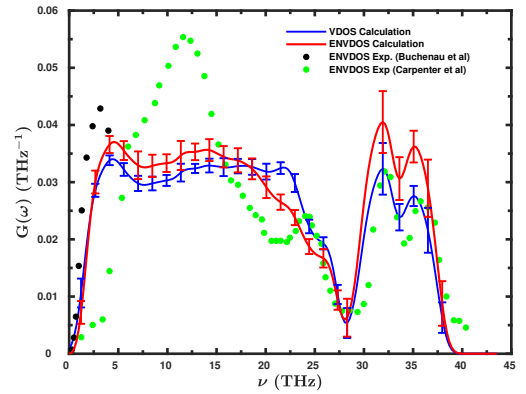


Figure 10: Averaged effective neutron density of states (red solid line) compared to the VDOS (blue solid line) and data from experiments in Ref.¹⁹ (green circles) and Ref.³⁶ (black circles)

is described as the boson peak³⁶ is not present in the experiment of Carpenter and Price¹⁹. The absence of this peak is interpreted by a lack of experimental resolution at low frequencies³⁷.

V. CONCLUSION

Using classical molecular dynamics simulations, we have generated an ensemble of ten small structural models of amorphous silica and the structural and dynamical properties have been investigated. All the structural properties of the models (the pair correlation functions, the O-Si-O and Si-O-Si bond-angle distributions and the elastic structure factor) show a good agreement with the experimental data. For the dynamical properties that we have computed, the overall agreement is good as well. However, at intermediate frequencies, around 12 THz, the calculated dynamical properties show a poor agreement with data from inelastic neutron scattering. This is especially true for the vibrational density of states, which confirms, in this frequency region, the deficiency of the BKS potential to reproduce accurately the vibrational properties, as is known from other studies.

Nevertheless, what can be learned from our study is that several properties, like the mean square-displacement, the vibrational density of states, and the dynamic structure factor, can be computed from an average over a few samples containing a small number of atoms (78), with an accuracy comparable to computations performed on larger systems, like the 648 atoms models investigated by Taraskin and Elliott¹³. When physical properties will have to be computed at the DFT level (at which the inadequacy of the vibrational spectrum around 12 THz is corrected), this represents an important computational time gain. Indeed, the computation of several physical properties (like the thermal conductivity or the diffusivity) scales as N^2 or N^3 , with

N the number of atoms in the computational cell. In our case, performing the computations over 10 small samples instead of one large one, allows reducing the computational time by a factor up to 50: this is not negligible.

VI. ACKNOWLEDGEMENTS

This work has been funded by the Institut Carnot "Chimie-Balard Cirimat" and the Institut Carnot "En-

ergie et Environnement de Lorraine". High Performance Computing resources were partially provided by the EXPLOR centre hosted by the University de Lorraine.

-
- ¹ M. Green, E. Gusev, R. Degraeve, and E. Garfunkel, *Journal of Applied Physics* **90**, 2057 (2001).
- ² T. Li, *Optical fiber communications: fiber fabrication* (2012).
- ³ J. R. G. Da Silva, D. G. Pinatti, C. E. Anderson, and M. L. Rudee, *The Philosophical Magazine: A Journal of Theoretical Experimental and Applied Physics* **31**, 713 (1975).
- ⁴ R. L. Mozzi and B. E. Warren, *Journal of Applied Crystallography* **2**, 164 (1969).
- ⁵ H. F. Poulsen, J. Neufeind, H.-B. Neumann, J. R. Schneider, and M. D. Zeidler, *Nuclear Instruments and Methods in Physics Research Section B: Beam Interactions with Materials and Atoms* **97**, 162 (1995).
- ⁶ J. Neufeind and K.-D. Liss, *Berichte der Bunsengesellschaft für physikalische Chemie* **100**, 1341 (1996).
- ⁷ N. M. Trease, T. M. Clark, P. J. Grandinetti, J. F. Stebbins, and S. Sen, *The Journal of Chemical Physics* **146**, 184505 (2017).
- ⁸ R. M. Van Ginhoven, H. Jónsson, and L. R. Corrales, *Physical Review B* **71**, 024208 (2005).
- ⁹ L. Giacomazzi, P. Umari, and A. Pasquarello, *Physical Review B* **79**, 064202 (2009).
- ¹⁰ P. Umari, X. Gonze, and A. Pasquarello, *Physical review letters* **90**, 027401 (2003).
- ¹¹ J. Sarnthein, A. Pasquarello, and R. Car, *Physical review letters* **74**, 4682 (1995).
- ¹² A. Pasquarello, J. Sarnthein, and R. Car, *Physical Review B* **57**, 14133 (1998).
- ¹³ S. Taraskin and S. Elliott, *Physical Review B* **56**, 8605 (1997).
- ¹⁴ W. Jin, P. Vashishta, R. K. Kalia, and J. P. Rino, *Physical Review B* **48**, 9359 (1993).
- ¹⁵ A. Pasquarello, *Physical Review B* **61**, 3951 (2000).
- ¹⁶ L. Giacomazzi and A. Pasquarello, *Journal of Physics: Condensed Matter* **19**, 415112 (2007).
- ¹⁷ B. Bhattarai and D. Drabold, *Journal of Non-Crystalline Solids* **439**, 6 (2016).
- ¹⁸ M. Arai, A. Hannon, A. Taylor, A. Wright, R. Sinclair, and D. Price, *Physica B: Condensed Matter* **180**, 779 (1992).
- ¹⁹ J. M. Carpenter and D. L. Price, *Physical Review Letters* **54**, 441 (1985), ISSN 0031-9007, URL <https://link.aps.org/doi/10.1103/PhysRevLett.54.441>.
- ²⁰ A. Hiramatsu, M. Arai, H. Shibazaki, M. Tsunekawa, T. Otomo, A. Hannon, S. Bennington, N. Kitamura, and A. Onodera, *Physica B: Condensed Matter* **219**, 287 (1996).
- ²¹ M. Nakamura, M. Arai, Y. Inamura, T. Otomo, and S. Bennington, *Physical Review B* **66**, 024203 (2002).
- ²² X. Yuan and A. N. Cormack, *Journal of non-crystalline solids* **319**, 31 (2003).
- ²³ B. W. H. van Beest, G. J. Kramer, and R. A. van Santen, *Physical Review Letters* **64**, 1955 (1990), URL <https://link.aps.org/doi/10.1103/PhysRevLett.64.1955>.
- ²⁴ P. Jund and R. Jullien, *Philosophical Magazine A* **79**, 223 (1999).
- ²⁵ M. Benoit, S. Ispas, P. Jund, and R. Jullien, *The European Physical Journal B-Condensed Matter and Complex Systems* **13**, 631 (2000).
- ²⁶ S. Le Roux and P. Jund, *Computational Materials Science* **49**, 70 (2010).
- ²⁷ P. Vashishta, R. K. Kalia, J. P. Rino, and I. Ebbsjö, *Physical Review B* **41**, 12197 (1990).
- ²⁸ D. Price and J. Carpenter, *Journal of non-crystalline solids* **92**, 153 (1987).
- ²⁹ A. Togo and I. Tanaka, *Scripta Materialia* **108**, 1 (2015).
- ³⁰ A. Pasquarello, J. Sarnthein, and R. Car, *Physical Review B* **57**, 14133 (1998).
- ³¹ M. Benoit and W. Kob, *Europhys. Lett.* **60**, 269 (2002), URL <https://doi.org/10.1209/epl/i2002-00346-7>.
- ³² F. L. Galeener, A. Leadbetter, and M. Stringfellow, *Physical Review B* **27**, 1052 (1983).
- ³³ K. Mizokami, A. Togo, and I. Tanaka, *Phys. Rev. B* **97**, 224306 (2018), URL <https://link.aps.org/doi/10.1103/PhysRevB.97.224306>.
- ³⁴ A. A. Maradudin, E. W. Montroll, G. H. Weiss, and I. Ipatova, *Theory of lattice dynamics in the harmonic approximation*, vol. 3 (1963).
- ³⁵ A. C. Wright and R. N. Sinclair, *Journal of non-crystalline solids* **76**, 351 (1985).
- ³⁶ U. Buchenau, M. Prager, N. Nücker, A. Dianoux, N. Ahmad, and W. Phillips, *Physical Review B* **34**, 5665 (1986).
- ³⁷ A. Wischniewski, U. Buchenau, A. J. Dianoux, W. A. Kamitakahara, and J. L. Zarestky, *Phys. Rev. B* **57**, 2663 (1998), URL <https://link.aps.org/doi/10.1103/PhysRevB.57.2663>.